Available online at www.sciencedirect.com
ScienceDirect
Journal of Nuclear Materials 375 (2008) 323–330
journal of nuclear materials
www.elsevier.com/locate/jnucmat

Characterization of oxide layers grown on D9 austenitic stainless steel in lead bismuth eutectic

P. Hosemann [a,b,*], M. Hawley [b], D. Koury [c], J.G. Swadener [b], J. Welch [c], A.L. Johnson [c], G. Mori [a], N. Li [b]

[a] CD Laboratory of Localized Corrosion, Montanuniversität Leoben, Franz-Josef Strasse 18, 8700 Leoben, Austria
[b] Los Alamos National Laboratory, P.O. Box 1663, Los Alamos, NM 87544, USA
[c] University of Nevada, 4505 S. Maryland Parkway, Las Vegas, NV 89154, USA

Received 4 September 2007; accepted 17 December 2007

Abstract

Lead bismuth eutectic (LBE) is a possible coolant for fast reactors and targets in spallation neutron sources. Its low melting point, high evaporation point, good thermal conductivity, low reactivity, and good neutron yield make it a safe and high performance coolant in radiation environments. The disadvantage is that it is a corrosive medium for most steels and container materials. This study was performed to evaluate the corrosion behavior of the austenitic stainless steel D9 in oxygen controlled LBE. In order to predict the corrosion behavior of steel in this environment detailed analyses have to be performed on the oxide layers formed on these materials and various other relevant materials upon exposure to LBE. In this study the corrosion/oxidation of D9 stainless steel in LBE was investigated in great detail. The oxide layers formed were characterized using atomic force microscopy, magnetic force microscopy, nanoindentation, and scanning electron microscopy with wavelength-dispersive spectroscopy (WDS) to understand the corrosion and oxidation mechanisms of D9 stainless steel in contact with the LBE. What was previously believed to be a simple double oxide layer was identified here to consist of at least 4 different oxide layers. It was found that the inner most oxide layer takes over the grain structure of what used to be the bulk steel material while the outer oxide layer consists of freshly grown oxides with a columnar structure. These results lead to a descriptive model of how these oxide layers grow on this steel under the harsh environments encountered in these applications.

1. Introduction

Lead bismuth eutectic (LBE) is considered an attractive coolant for various nuclear applications. Its low melting point, low reactivity, low vapor pressure, low viscosity, good gamma shielding, and high neutron yield make LBE cooled reactors and spallation sources good candidates for advanced energy systems. The main difficulty in using LBE as a coolant effectively lies in understanding and controlling the corrosion of candidate structural materials in LBE. It is believed [1,2] that protective oxide layers can be formed on LBE-exposed steel in order to prevent further corrosion, but to ensure that oxide layers formed on steels can last at the system operation conditions (high flow rate, high temperature, etc.) for a long period of time (40+ years for reactors), their structure and growing mechanism must be understood. Here micro and nanoscale techniques are used to investigate the structure and properties of the oxide layer formed on D9 stainless steel (SS) in an LBE environment at 550 °C. The goal of this investigation is to get a better understanding the oxide layers and their growth mechanism, which will help model their growth more accurately.

2. Experiment and post corrosion analyses

Tubes of D9 SS were exposed to LBE in the liquid LBE loop system at the Institute of Physics and Power

* Corresponding author. Address: Los Alamos National Laboratory, P.O. Box 1663, Los Alamos, NM 87544, USA. Tel.: +1 505 629 9893; fax: +1 505 667 7443.
E-mail address: peterh@lanl.gov (P. Hosemann).

0022-3115/$ - see front matter © 2008 Elsevier B.V. All rights reserved.
doi:10.1016/j.jnucmat.2007.12.005

Engineering (IPPE) in Obninsk, Russia. The nominal composition of this material is 13.6% Cr, 13.6% Ni, 2.1% Mn, 1.11% Mo, 0.85% Si, 0.04% C, and 0.30% Ti (by weight) with the balance in Fe. The titanium serves to form voids and dislocations in the austenite matrix by forming TiC precipitates. The voids provide sinks for point defects induced by exposure to fluxes of high energy particles to help moderate swelling and thermal expansion in nuclear environments [3]. The D9 SS tube was exposed to 2 m/s flowing LBE with 10^{-6} wt% oxygen content at 550 °C for 1000 h, 2000 h, and 3000 h. The LBE flow direction was parallel to the tube length. After exposure the tubes were cut in 5 mm long pieces and mounted in Epoxy cold mount. The mounted samples were then polished using colloidal silica on a Buehler Vibromet2 polisher prior to characterization. The polishing step provides a very flat, smooth surface, which is required for nanoindentation. These cross section samples were analyzed using atomic force microscopy (AFM), magnetic force microscopy (MFM), scanning electron microscopy (SEM), and wavelength-dispersive X-ray spectroscopy (WDS).

2.1. AFM and MFM measurements

AFM characterization of the structure and properties of the various layers was performed at Los Alamos National Laboratory (LANL) using a Veeco Metrology Nanoscope IIIa controller and D3000 microscope. The tip used was a commercial silicon Tapping Mode™ cantilever with a magnetic CoCr coated tip. The scan rate was generally $\leqslant$0.4 Hz for a 40 μm × 40 μm scan area (lower magnification) and adjusted to a higher frequency for smaller images. The resonance frequency of this tip was ~65 kHz. Topographic and corresponding magnetic images were taken simultaneously at the same location. In some cases a corresponding phase image was also collected.

2.2. Nanoindentation measurements

The Nanoindentation measurements were done at LANL using a Hysitron Tribo® indenter equipped with a multi-range nanoprobe, an optical microscope, and an AFM. The indenter uses a diamond Berkovich indenter tip. To take into account the nanoindentation size effect [4] (which shows higher hardness as the indents gets smaller) the system was operated in displacement mode (displacement was set at 200 nm). This allowed direct comparison between indents within the array of indents. The loading rate was 10 nm/s, the holding time was 10 s, and the unloading rate was 10 nm/s. An array of 6 × 14 indents was made on each sample. Each row of 6 indents was parallel to the original sample surface. The indents were spaced 4 μm apart to minimize interference. Before and after performing the array of indents, a contact mode image AFM was taken using the indenter tip to determine the location of the indents relative to the oxide layers and underlying D9 SS.

2.3. SEM and WDS measurements

SEM and WDS investigations were performed at the University of Nevada, Las Vegas using a JEOL 5610 scanning electron microscope for SEM and a JEOL JXA-8900R Electron Probe Microanalyzer for WDS. Elemental maps and linescans were obtained using EDX or WDS in those cases where spectral overlap was a problem (e.g., in a typical EDS spectrum, Mn Kα and Kβ peaks overlap the Cr Kβ and Fe Kα, respectively). The acceleration voltage in both the SEM and the Electron Probe was 15 kV, and both were operated at a working distance of 20 mm.

3. Results

3.1. SEM and WDS

The SEM and WDS measurements revealed two different types of oxidation/corrosion regions. One region consisted of a thin, chromium rich oxide layer while the other had a thick, duplex oxide layer structure. The thicknesses of the two oxide layers composing the duplex outer oxide layer seem to increase with exposure time (Table 1). The results shown there are gained from SEM analysis. The values given are average values of 5–7 measurements. The SEM images revealed that the outer oxide layer thickness stayed nearly constant while the inner oxide layer thickness increased with exposure time. It can also be seen in Fig. 2 that the previous steel grain boundaries are still visible in the inner oxide layer. The bright spots in Fig. 2(a) are the remaining LBE. Previous work reported the EDS spectrums [12]. Note that the LBE is only found within the outer layer.

The WDS line scans reveal that the outer oxide layer is almost exclusively Fe and O (Fig. 3). The ratio between Fe and O is 70 wt% Fe and 30 wt% O. This is consistent with the atomic weights for magnetite (72.4% Fe and 27.6% O) and hematite (69.9% Fe and 30.1% O). However, under these conditions (temperature, oxygen concentration) hematite is thermodynamically not stable and previous work confirms the existence of magnetite [2,5]. The inner oxide layer is in general Cr, Ni, Mn, and Si enriched with respect to the native steel, most notably at the grain boundaries. The composition found agrees very well with previous results under similar oxidation conditions [2] (at 400 °C and 550 °C exposure in IPPE loop for 1027 h, 2000 h, 3027 h with 3–4 × 10^{-5} wt% O in the LBE). At

Table 1
The oxide layer thickness as a function of exposure time

Exposure time (h)	Inner layer thickness (μm)	Outer layer thickness (μm)	Remarks
1000	5–15	5	Rough metal-oxide
2000	5–15	5	
3000	5–20	5–10	

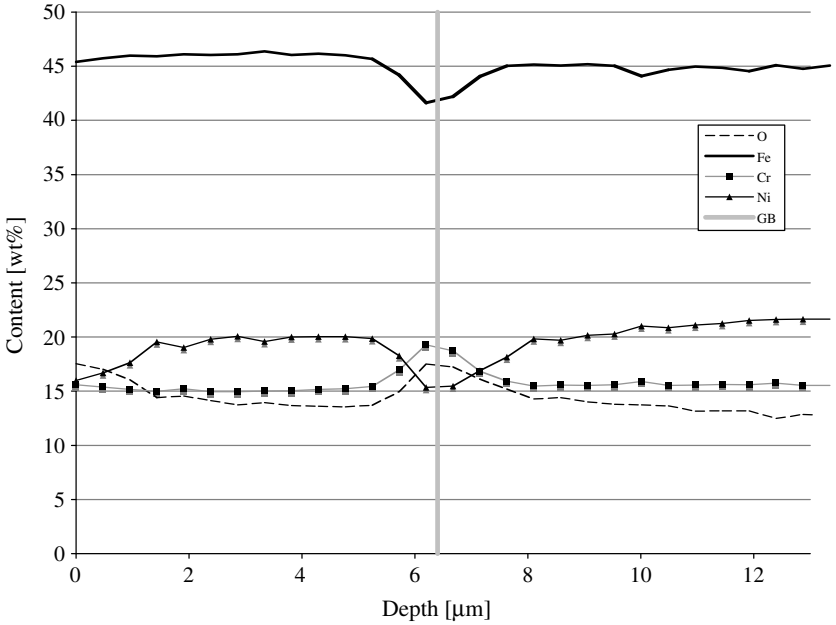

Fig. 1. WDS linescan across an inner oxide grain boundary.

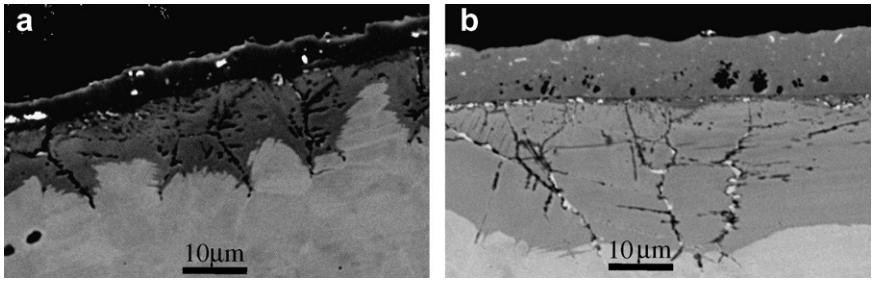

Fig. 2. Back scattered SEM image of the D9 after (a) 1000 h and (b) 3000 h exposure to LBE.

the interface between the inner and outer layers a thin (<1 μm thick) layer with a slight Cr enrichment was found.

3.2. Nanoindentation and AFM

The nanoindentation results of the samples cross-sections are presented in Figs. 4–6. The hardness and *E*-modulus values presented are always the average of 6 indents in a row, all at the same distance from the surface (see Fig. 7). These average values do not reflect the variation in properties of different locations (grain boundary, within grain, close to interfaces, etc.) and, therefore, represent only average behavior with a maximum experimental uncertainty of ±1.5 GPa for the hardness and ±40 GPa for the *E*-modulus. But it can be seen in the nanoindentation depth profiling that the *E*-modulus decreases on all of the samples from the steel (190–220 GPa) to the outer oxide layer (50–150 GPa) in a step like function. This has also been observed and previously reported in the literature [14]. The *E*-modulus of the outer and inner oxide layers increases with higher exposure time but never reaches the value of the bulk steel. At the same time the hardness increases within the oxide layer to about 12–14 GPa.

AFM characterization was performed after nanoindentation. In general these measurements were performed at the same location where the nanoindentation was conducted. These measurements are similar to what was reported in [13]. Fig. 7 presents topography and magnetic force images of the 3000 h LBE-exposed sample. In both images (topographical (a) and MFM (b)) 4 different structural or magnetic layers can be identified. Fig. 8 shows a higher magnification of the locations marked in Fig. 7. In Figs. 7 and 8 the outer layer, marked 'layer 1', has a very fine globular grain structure (120–400 nm grain size) while the outer layer 2 has much larger and strongly oriented grain (800–1200 nm width and 2500 nm–3500 nm length). Both outer layers have a large number of small pores (10–120 nm in size). It seems at this point that the pore density is higher in outer layer 1 than in outer layer 2. Inner layer 3 can not be distinguished using the topography image. It only appears in the MFM image and corresponds to the Cr enriched location found using WDS. Inner layer 4 has a similar grain structure as the bulk steel (see Figs. 7 and 9). Fig. 9(a) presents a detailed image of the inner oxide layers. The cracks at grain boundaries and the pores (10–50 nm in size) can be seen in inner layer 4. A fine

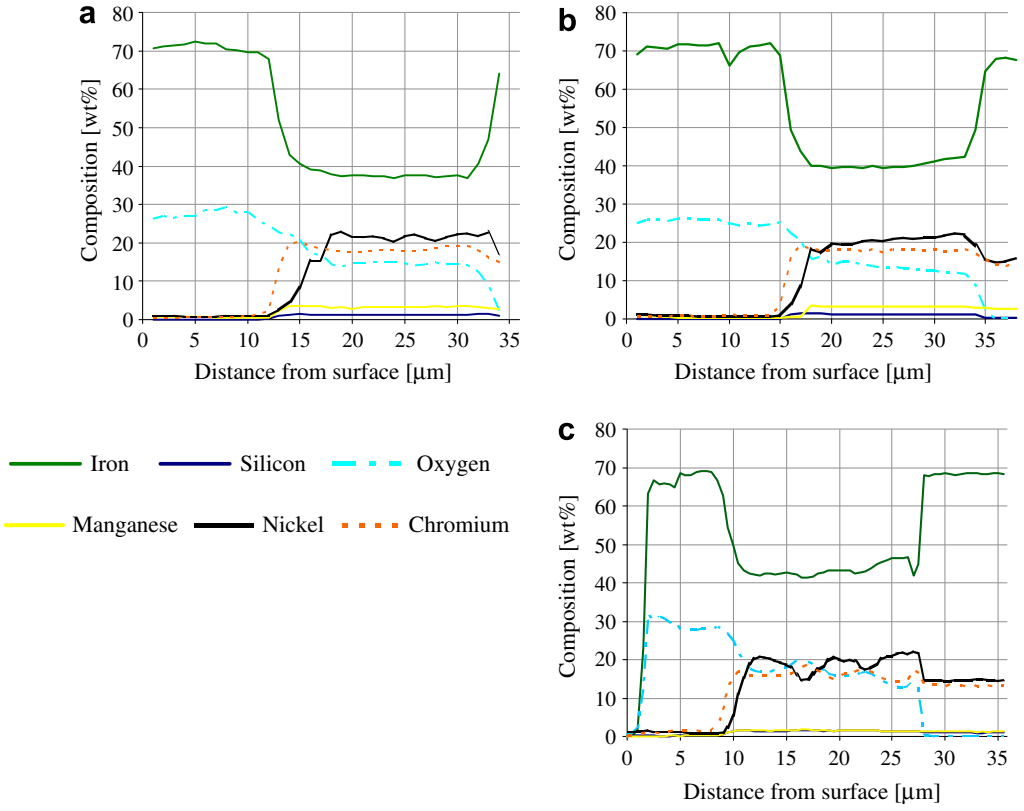

Fig. 3. WDS line scans through oxide layers of steel D9 exposed to LBE at 550 °C after (a) 1000 h, (b) 2000 h, and (c) 3000 h.

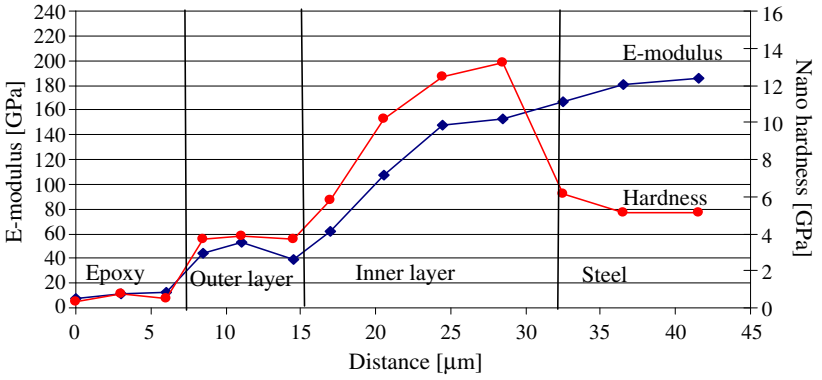

Fig. 4. Results of the nanoindentation performed of D9 after 1000 h in LBE.

structure within the grains of the inner layer was found (20–100 nm feature size) as it is shown in the high resolution AFM image presented in Fig. 9(b).

4. Discussion

The double-layered oxide regions revealed (using SEM/WDS) an appearance where the inner layer maintains the grain structure of the steel while the outer layer does not. In addition LBE was found within the outer layer using SEM/EDS as it can be seen in Fig. 2. The bright spots in the outer oxide layer are LBE. This supports the theory that the outer layer grows by the diffusion of steel elements (primarily iron) from the metal towards its surface (cation diffusion) while the inner layer grows by oxygen diffusion from the LBE into the steel (anion diffusion) [10]. The WDS results show that inner layers 3 and 4 consist of a mixed oxide. Also a small Cr enrichment can be seen in inner layer 3. Detailed TEM analysis would be needed to investigate further the crystallographic nature of these mixed oxide layers. A line scan across an inner oxide layer grain boundary (Fig. 1) shows a clear Cr and O enrichment at the grain boundary. This supports the assumption that O and Cr use the grain boundary as a fast diffusion path and Cr oxide and/or Cr–Fe spinel is formed there first while the excess amount of Fe is diffusing towards the outer

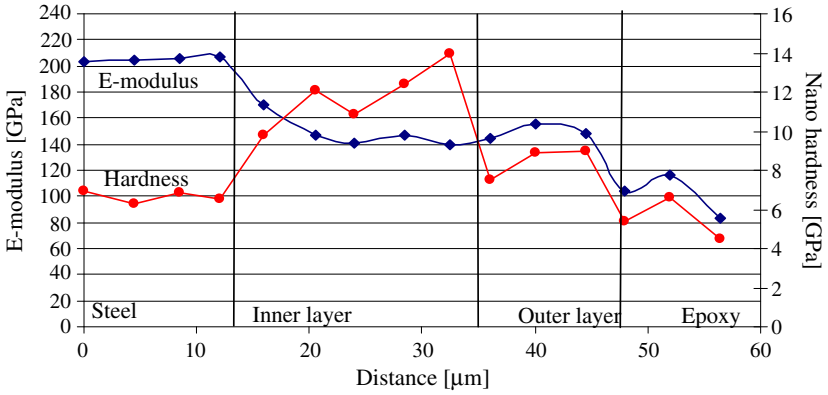

Fig. 5. *E*-modulus and nano hardness results of D9 after 2000 h in LBE.

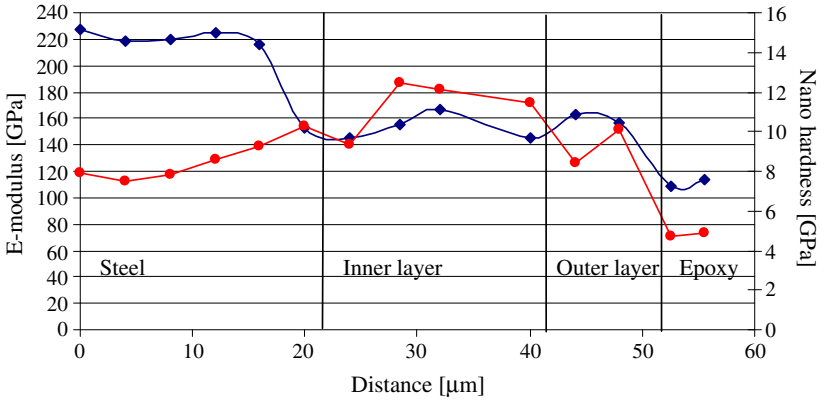

Fig. 6. Nano hardness and *E*-modulus results of D9 after 3000 h in LBE.

oxide layer. Also worth noting is the depletion of Ni in the oxide grain boundaries, despite an overall Ni enrichment in the inner layer. The amount of minor alloying elements like Si, Mn, and Mo are elevated in the inner oxide layer as well. Using AFM, MFM and nanoindentation the previous steel grain boundaries in the oxide layer can be observed as well (Fig. 7). The AFM reveals that the area surrounding the grain boundaries have a large amount of pores, cracks and precipitates. By carefully analyzing the nanoindents performed on the D9 3000 h sample and looking at each location of the indents with respect to their location within grains or near a grain boundary, it was found that the indents placed on or near the grain boundaries of the steel measured higher hardness than the indents in the steel grain. This is expected according to [6]. The indents placed near or in an oxide grain boundary measured significantly lower hardness (2 GPa) than the indents inside the grain (Fig. 10). Similar phenomena were observed [7] on fully yttria stabilized zirconia (F-YSZ). In contrast to the measurements in F-YSZ on large grains [7] no pop in (a sudden displacement change by unchanged load) phenomenon was found here. It was also found [7] that small grain structured materials do not show pop in. Since the AFM measurements performed here revealed a large number of pores (within the grain and on grain boundaries) and a small substructure within the large grains it appears that these features lead to material behavior as seen for a fine grained material [7]. The MFM measurement reveals that close to the interface between the inner and outer layers, the magnetic structure changes from moderate polarization to no out-of-plane polarization. This 'magnetic denuded' zone has a thickness of ~1 µm and is labeled as inner layer 3. The fact that the 1 µm thick inner layer 3 is surrounded by strong magnetically polarized zones (inner layer 4 and outer layer 2) can exclude a scanning artifact. So far it is not entirely clear what causes the different magnetic structure within the inner oxide layer. No structural change (topographical image) was observed. Only the WDS reveals a slight Cr enrichment in this area. It is possible that this slightly Cr enriched non magnetic layer is the initial oxide layer formed during the first few hours of exposure to LBE.

The WDS measurements show that the outer layer consists homogeneously of Fe_3O_4, however, the AFM/MFM (Fig. 8) and nanoindentation (Figs. 4–6) data clearly reveal that the outer layer actually consist of 2 layers (outer layer 1 and outer layer 2) that differ in grain structure (outer most oxide layer 1 has small round shaped grains and outer layer 2 has larger and more oriented grains) and magnetic structure (outer layer 1 has a weaker magnetic structure than outer layer 2). Due to the fact that the outer layer on the 1000 h sample is only ~5 µm thick the detailed

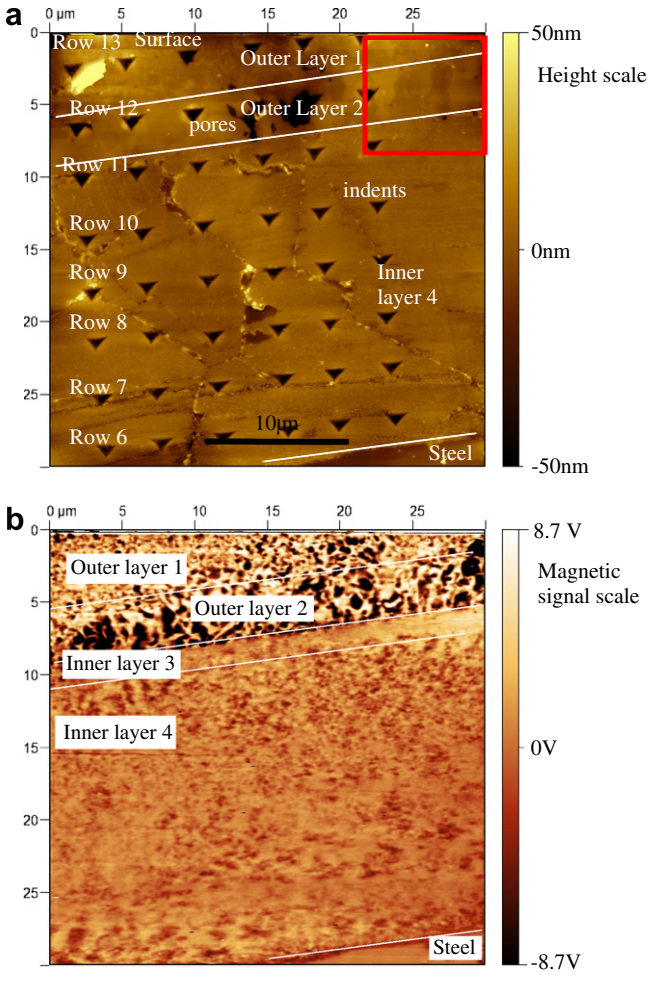

Fig. 7. AFM topography image (a) and magnetic force image (b) of D9 after 3000 h in LBE. The array of nano indents is marked as well as the identified oxide layers.

nanoindentation analyses were only done on the 2000 h and 3000 h sample. The data revealed that the indents located in outer layer 1 always have higher hardness than the indents in the outer layer 2 (Figs. 4–6). Post indentation depth analyses using cross section line scans in the AFM off-line analyzing software, reveal that outer layer 1 has a smaller residual depth than outer layer 2. This is in agreement with the nano hardness measurements where the outer layer 1 appears to be harder than outer layer 2. Therefore, the finer grains have a higher hardness than the larger grains in these oxide layers. The MFM measurements also show a much stronger magnetic contrast in the larger grained material than in the smaller grained material. Since there is no obvious chemical difference between outer layer 1 and outer layer 2 (both seem to be magnetite) it is assumed here that this effect comes from the difference in grain structure.

Looking at all three samples (1000 h, 2000 h and 3000 h) it can be seen that the inner oxide layer is in general thicker than the outer oxide layer. This can result from either different growth rates or simply the loss of outer layer material to the LBE. At this point it is not entirely clear which of this two possible cases is true, but based on the fact that LBE was found inside the outer layer area and that Fe diffusion is, in general, faster than O diffusion [9,11], it is suggested that the thinner outer layer is simply losing material to the LBE flow.

Fig. 11 presents a schematic drawing of the oxide layer growth process in contact with LBE. In the first stage a very thin layer of a Cr–Fe–O phase forms on the surface. This would correlate with the presence of the thin 'denuded' magnetic zone observed in the MFM images and to the slight Cr enrichment at the interface between the inner and outer layers. Also no Ni was found in inner layer 3 which might suggest that the Ni has been leached out (Ni has the highest solubility in LBE) from the surface at initial exposure to LBE. At this point it is not clear if this phase is Cr_2O_3 or a Fe–Cr spinel since no speciation measurements (XPS, XRD, TEM, Raman scattering) were performed yet. During exposure to LBE at elevated temperatures the Fe starts diffusing through this first layer

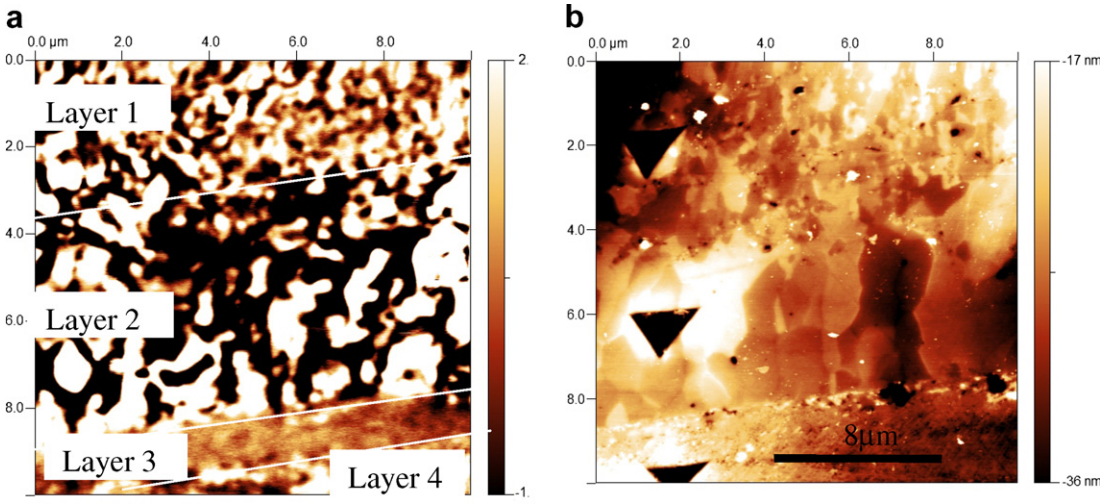

Fig. 8. Left side, magnetic force microscopy image (a). Right side corresponding topography image of the same location (b).

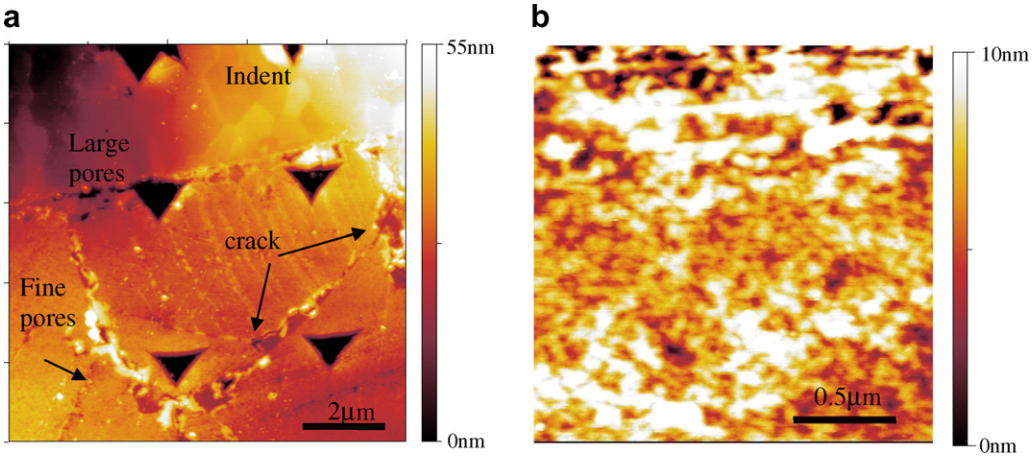

Fig. 9. AFM topography image of the inner layer of the sample D9 3000 h (a). AFM topography image of the inner layer of the sample D9 3000 h within the grain (b).

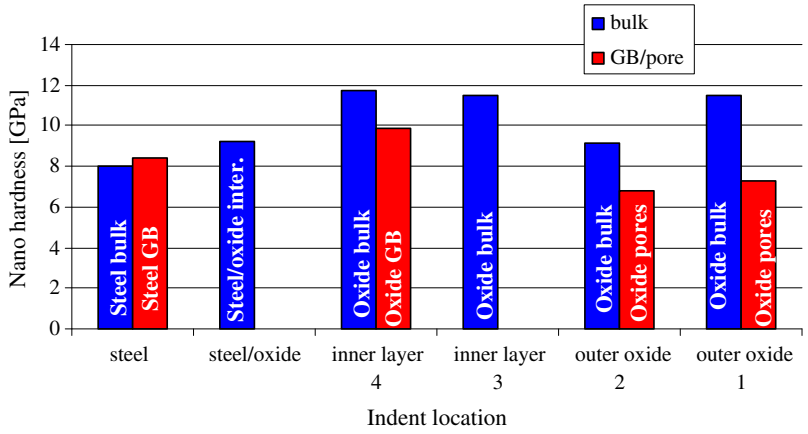

Fig. 10. Nano hardness dependence on the indent location (indent inside the grain or at a grain boundary or at a pore).

towards the surface and forms a new Fe_3O_4 layer on the surface. This new layer grows in contact with the LBE, trapped some LBE within pores, which can act as fast transport paths for O and may act later as crack initiators. Since grain boundaries in the steel are fast diffusion paths (pipe diffusion) the process starts there first in the steel. The vacancies and pores caused by the missing Fe within the steel make it easier for O to diffuse into the material [10]. Again the grain boundaries act as fast diffusion paths for the O. Assuming this mechanism is true and there is a sufficient oxygen supply through the flowing LBE the corrosion rate limiting factor is the Fe diffusing toward the surface. Since the crystal structure and different phases are not clearly identified to this point corrosion rate estimations based on the structural findings here are not possible. The fact that Cr is never found in the outer layer but is

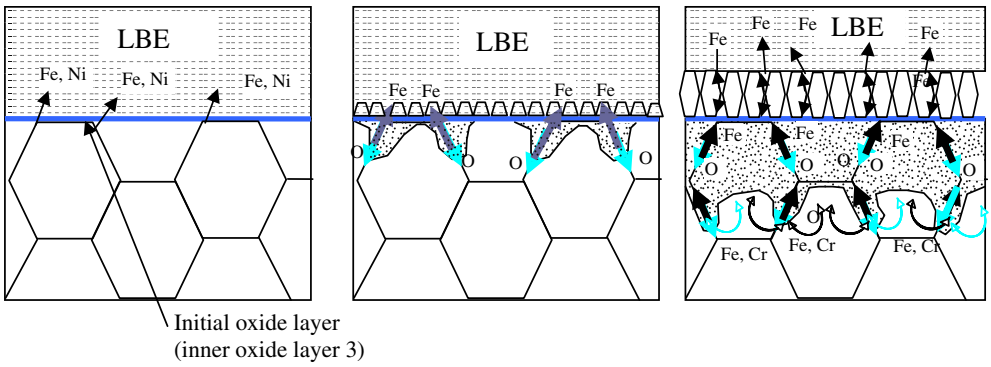

Fig. 11. Schematic drawing presenting the oxide layer growth mechanism proposed here.

found enriched at the grain boundaries leads to the assumption that Cr diffuses from the grain interior to the grain boundary as well. However, as soon as Cr contacts O it forms either Cr_2O_3 or $(Fe,Cr)_2O_4$, which are both very stable phases. Therefore, the Cr remains in this phase and does not move any further. The other explanation is that the Cr forms Cr rich stable oxides as soon as it is in contact with the O and the excessive amount of Fe can diffuse to the surface leaving a porous Cr rich area surrounding the fast diffusion paths (grain boundaries) behind. The fine structure within the grains of inner layer 4 might be due to local element segregation or to the fact that the oxide formation starts at multiple nucleation sites simultaneously and leads to a sub grain structure.

The fact that the larger grains in the outer layer 2 were found in the 1000 h, 2000 h and 3000 h specimen, implies that the large grains are not a result of a grain coarsening process over time. At this point it is not entirely clear why the grain structure changes from the large grains into the small grains after the outer oxide layer reaches a thickness of 4–6 μm, but here it is suggested that the change to smaller grains is due to the longer diffusion path for the Fe towards the surface. If nucleation is occurring at a constant rate, less Fe arrives at the surface per nucleation event forming smaller grains. It can be seen that the residual indentations in the oxide layers are triangle shaped without any deformation or much cracking. This indicates that internal stress in the oxides is low. But it is known from Pilling and Bedworth [8] that the oxide has a much larger volume than the steel (fcc is close packed) and, therefore, should cause compression stress in the oxide layer and tensile stress in the steel. It may be that the pores compensate for this stress.

5. Conclusion

- The D9 steel forms 4 different layers on its surface during exposure to LBE. These are:
  - o Outer layer 1, a fine (sub micron size) grained Fe_3O_4 layer. No distinguished grain orientation was observed. This layer has a strong magnetic polarization.
  - o Outer layer 2, a larger (micron size) grained Fe_3O_4 layer. The grains are elongated in the growing direction. This layer has the strongest magnetic polarization.
  - o Inner layer 3, (only visible in the MFM measurements) has no magnetic polarization. The WDS data reveal a slight Cr enrichment at the very same location of the oxide layer, which indicates a higher Cr content phase.
  - o Inner layer 4, shows the same grain structure as the bulk steel. The grain boundaries are weak and cracked, and show some precipitates. The magnetic structure is relatively weak. The WDS line scan across these grain boundaries show Cr and O enrichment which leads to the possibility that the particles found there might be a Cr rich phase.
- All oxide layers showed some porosity. These pores seem to be responsible for the low hardness and *E*-modulus values (compared to dense oxides) in the oxide layers.
- It appears that the inner oxide layer growth within the bulk steel is driven by diffusion of Fe and O along the existing steel grain boundaries.
- Duplex oxide thickness increases with exposure time.

Acknowledgements

This work was performed in part at the Center for Integrated Nanotechnologies, a US Department of Energy, Office of Basic Energy Sciences user facility at the Los Alamos National Laboratory. The Los Alamos National Laboratory is operated by Los Alamos National Security, LLC, for the National Nuclear Security Administration of the US Department of Energy under contract DE-AC52-06NA25396. We would also like to thank IPPE in Obninsk, Russia for supplying the samples. The authors would like to thank Dr Robert Fairhurst, staff scientist, Geoscience Department, UNLV, for assistance using the Electron Probe Microanalyzer.

References

[1] J. Zhang, N. Li, Y. Chen, A.E. Rusanov, J. Nucl. Mater. 336 (2005) 1.
[2] H. Glasbrenner, J. Konys, G. Mueller, A. Rusanov, J. Nucl. Mater. 296 (2001) 1.
[3] A. Banerjee, S. Raju, R. Divakar, E. Mohandas, G. Panneerselvam, M.P. Antony, J. Nucl. Mater. 347 (2005) 20.
[4] F. Schulz, H. Hanemann, Z. Metallkd. 33 (3) (1941) 124.
[5] T. Furukawa, G. Müller, G. Schumacher, A. Weisenburger, A. Heinzel, F. Zimmermann, K. Aoto, J. Nucl. Sci. Technol. 41 (3) (2004) 265.
[6] T. Ohmura, K. Tsuzaki, F. Yin, Mat. 46 (9) (2005) 2026.
[7] J. Lian, J.E. Garay, J. Wang, Scripta Mater. 56 (2007) 1095.
[8] N.B. Pilling, R.E. Bedworth, J. Ins. Met. 29 (1923) 529.
[9] R.E. Lobnig, H.P. Schmidt, K. Hennesen, H.J. Grabke, Oxid. Met. 37 (1992).
[10] M. Saito, H. Fururya, M. Sugisaki, J. Nucl. Mater. 135 (1985) 11.
[11] J. Robertson, Corros. Sci. 29 (1989) 11.
[12] A.L. Johnson, D. Koury, J. Welch, T. Ho, S. Sidle, C. Harland, B. Hosterman, U. Younas, L. Ma, J.W. Farley, in: Proceedings for IV International Workshop on Materials for HLM Cooled Reactors and Related Technologies, J. Nucl. Mater., 2007.
[13] P. Hosemann, M. Hawley, G. Mori, N. Li, S.A. Maloy, in: Proceedings for IV International Workshop on Materials for HLM Cooled Reactors and Related Technologies, J. Nucl. Mater., 2007.
[14] P. Hosemann, J.G. Swadener, J. Welch, N. Li, in: Proceedings for IWSMT-8, J. Nucl. Mater., 2008.